World Academy of Science, Engineering and Technology
International Journal of Mechanical and Mechatronics Engineering
Vol:13, No:3, 2019

A Multigrid Approach for Three-Dimensional Inverse Heat Conduction Problems

Jianhua Zhou, Yuwen Zhang

***Abstract*—**A two-step multigrid approach is proposed to solve the inverse heat conduction problem in a 3-D object under laser irradiation. In the first step, the location of the laser center is estimated using a coarse and uniform grid system. In the second step, the front-surface temperature is recovered in good accuracy using a multiple grid system in which fine mesh is used at laser spot center to capture the drastic temperature rise in this region but coarse mesh is employed in the peripheral region to reduce the total number of sensors required. The effectiveness of the two-step approach and the multiple grid system are demonstrated by the illustrative inverse solutions. If the measurement data for the temperature and heat flux on the back surface do not contain random error, the proposed multigrid approach can yield more accurate inverse solutions. When the back-surface measurement data contain random noise, accurate inverse solutions cannot be obtained if both temperature and heat flux are measured on the back surface.

***Keywords*—**Conduction, inverse problems, conjugated gradient method, laser.

I. Introduction

LASER energy deposition into and the resulting temperature in a target are two of the key parameters for any laser-material interaction problem. The conventional temperature sensors cannot be used to directly measure the surface temperature because the sensors can interfere with the laser beam, which causes damage of the sensor. While remote sensing with radiation pyrometers or infrared cameras has been employed to measure the surface temperature, the measurement may not be reliable, particularly for composite targets or painted metal target because smoke and outgassing, resulting from resin pyrolysis and fiber charring or burning of paint, block thermal radiation from the front surface. Laser energy absorbed by a target can be estimated with the measured reflectance and transmittance. However, the accuracy of such measurement is often questionable due to the material anisotropy, surface roughness, smoke/outgassing, and fiber charring of the target. The inaccuracy can be worsened by non-uniform, skew beam profiles. For these circumstances, however, the heated surface temperature can be determined indirectly by solving an inverse heat conduction problem (IHCP) [1]-[3] based on the transient temperature and/or heat flux measured on the back surface. Unknown boundary conditions can be recovered and thermophysical properties can be estimated via solution of IHCP [4]-[8]. Zhou et al. [9] estimated the front surface heating conditions of metallic and composite targets based on the measured temperature and heat flux with temperature-dependent thermophysical properties using a 1-D model.

Zhou et al. [10] developed well-posed 3-D inverse heat transfer (IHT) models based on Conjugated Gradient Method (CGM) for metal target for the cases of known heat source location [11]. The capability of 3-D IHT model for metal was extended to handle dynamic and irregular laser beam profile [12]. The CGM-based IHT model was extended to be able to handle different number of sensors in the array and heat conduction in the substrate [13]. The front surface temperature of a locally heated plate with temperature-dependent conductivity was also estimated via Kirchhoff transformation [14]. Zhou et al. recovered the front surface temperature of the composite target subject to high-energy laser irradiation via solution of a three-dimensional IHT problem with pyrolysis and outgassing effects [15]. The progresses made by the authors' research group on 3-D IHT modeling for metallic and composite targets under high-energy laser interaction was reviewed in [16].

There is always trade-offs between accuracy and efficiency for IHCP. While large grid number and small mesh size result in accurate results, the computational cost will also increase. In this paper, a two-step multigrid approach for three-dimensional IHCP is proposed and its capability is demonstrated.

II. Physical Model and Multiple Grid System

Consider a 3-D object with dimension $AL \times AM \times AN$ as shown in Fig. 1. The rectangular coordinate system O-xyz is also shown. Initially, the object is uniform at temperature T_0. From $t = 0^+$, the front surface ($x = 0$) is subjected to a laser beam irradiation with irregular spot. The purpose of the inverse algorithm is to recover the observed heat flux $q_1(y, z, t)$ at front surface (x=0) based on the temperature and heat flux measurement data at back surface (x=AL).

In field cases, the spot of the laser beam is irregular and the spot location is unknown before solving the inverse problem. A sensor array including a large number of sensors may be needed to search for the location of the laser beam. To reduce the number of sensors required without loss of inverse accuracy, a two-step algorithm is designed to alleviate the difficulty of the problem.

In the first step, the 3-D inverse heat conduction simulation is performed based on a coarse and uniform grid system using

Jianhua Zhou was with University of Missouri, Columbia, MO 65211, USA. He is now with Carrier Corporation, Syracuse, NY 13057, USA (e-mail: jnhzhou@gmail.com)

Yuwen Zhang is with the University of Missouri, Columbia, MO 65211, USA (corresponding author, phone: 573-884-6936; fax: 573-884-5090; e-mail: zhangyu@missouri.edu).

the approaches described in our previous works [11], [12]. In the second step, a multiple grid system is devised to reflect the different temperature responses caused by the different intensities of laser heating flux applied on the front surface.

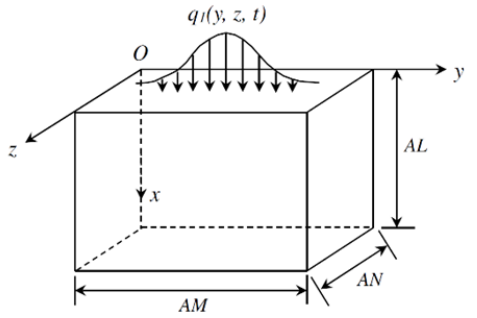

Fig. 1 Physical model

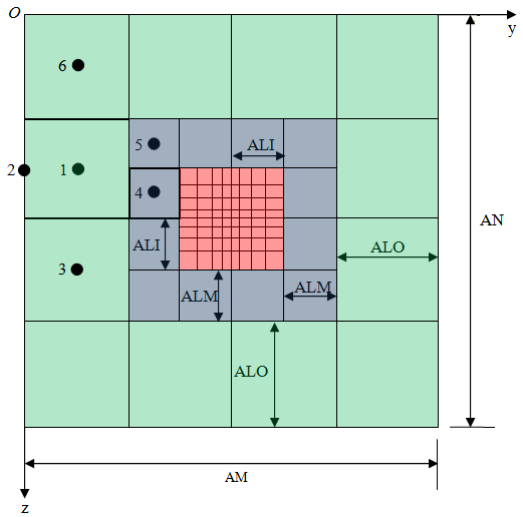

Fig. 2 Multiple grid system on *yOz* plane

In the multiple grid system, the mesh in the *x*- direction is still uniform, but the mesh on *yOz* plane is non-structured and non-uniform, which is depicted in Fig. 2. There are three regions in the *yOz* mesh, which are marked with different colors. The red color region with small grid size, which is located at the center, is used to capture the drastic temperature rise at the laser spot center. The green color region with large grid size is located at the peripheral area of the *yOz* plane. A blue color region comes between them. As can be seen, the grid size gradually increases from the center region to the peripheral region. Such a non-structured mesh is chosen based on the feature of laser beam profile, which usually has its maximum intensity at the center and gradually attenuates in regions away from the center.

The sizes of the three regions shown in Fig. 2 can be flexibly adjusted. The mesh in the red color region is structured but non-uniform. The grid size and the grid number in this region can be specified at will. The meshes in the blue and green color regions are non-structured. The lengths in the blue color and green color regions, ALM and ALO, can also be changed arbitrarily. A combination of these sizes can give a variety of mesh patterns, which is expected to be able to meet the needs in real cases.

It is worth pointing out that the lines shown in Fig. 2 are the boundaries of control volumes. The grid points are located at the center of each control volume. For a structured grid system, as we used before [11], the number of the neighboring points of each grid point is 4 on the 2-D yOz plane. But for a non-structured grid system shown in Fig. 2, the number of the neighboring points of each grid point on yOz plane may be more than 4 on the yOz plane. For instance, for the grid point 1, there are 5 neighboring grid points, i.e., grid points 2, 3, 4, 5, and 6. Special care is used to derive the coefficients related to grid points 4 and 5 for the discretization equation at grid point 1. Energy balance needs to be maintained in deriving these coefficients.

The above-described multiple grid system is incorporated into the previously developed 3-D CGM inverse model [11], [12]. Two cases are considered. One case is that the front-surface temperature is recovered based on the temperature *and* heat flux measurements on the back surface. The other case is that the front-surface temperature is recovered based on the temperature measurement *only* on the back surface. For the latter case, the boundary condition of the back surface is set to be thermally insulated.

III. Simulation Parameters

Stainless steel is taken as the simulation material. The dimension of the 3-D object considered is $AL \times AM \times AN$ = 3 mm×120 mm×120 mm. Initially, the object is at a uniform temperature of 300 K. The density of the 3D object is considered to be constant and uniform: ρ=7570 kg/m^3. However, the thermal conductivity and specific heat are temperature-dependent as follows:

$$k(T) = 12.45 + T \cdot (1.140 \times 10^{-2} + 2.517 \times 10^{-6} T) \quad (1)$$

$$c_p(T) = 470 + 0.175 \cdot T \quad (2)$$

where the units of temperature T, thermal conductivity $k(T)$ and $c_p(T)$ are K, W/(m•K) and J/(kg•K), respectively.

The heating flux on the front surface is assumed to be in the following form:

$$q''(y,z,t) = \alpha \cdot q_0'' \cdot (1 + \sin(2\pi ft) \cdot \exp\{-0.5[\cos\theta(y - y_c) + \sin\theta(z - z_c)]^2 / S_y^2 - 0.5[-\sin\theta(y - y_c) + \cos\theta(z - z_c)]^2 / S_z^2\} \cdot \quad (3)$$

where α is the surface absorptivity, α =0.05; q_0'' is the maximum heat flux at the center of the heating flux spot, q_0'' =10,000 W/cm^2; $(0, y_c, z_c)$ is the coordinates of the heating flux spot; S_y, S_z and θ are parameters for defining heating flux spot shape, S_y=22 mm, S_z=10 mm, $\theta = \pi / 6$; f is the frequency of the sinusoidal component of the heating flux.

The temperature and/or heat flux measurement data on the back surface are numerically obtained by solving a direct problem. Such "measurement data" are then superimposed by a random error item which follows a Gaussian distribution with certain standard deviation. The random noise in the back-surface measurement data (temperature and/or heat flux) is reduced using traditional Moving Window Average method.

The sensors measure the back-surface temperature at a sampling interval of 0.005 s, which is also the time step used in the finite difference simulation. Each simulation case is conducted from 0 s through 1 s.

IV. Results and Discussions

A. Measurement Data without Random Errors

1) First step: Identify the Location of Laser Irradiation in a Coarse Grid System

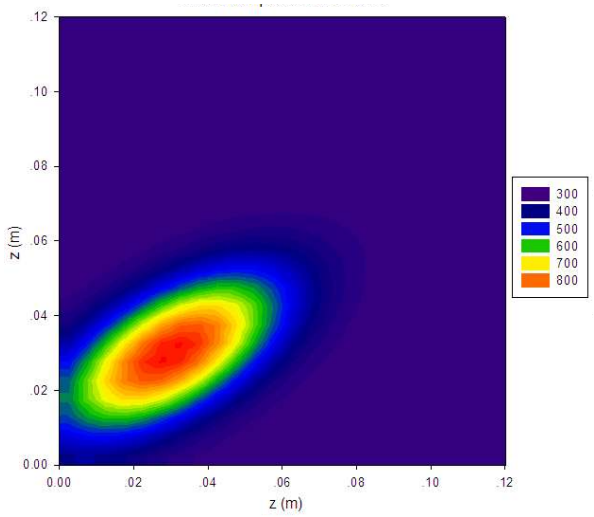

(a) The exact solution of the temperature rise at 1.0 s

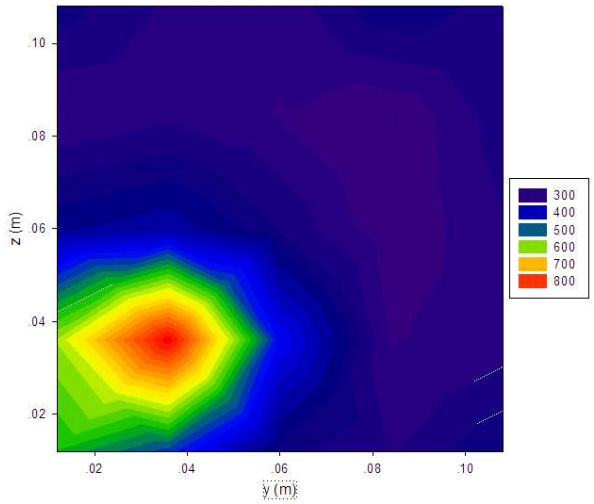

(b) The inverse solution of the temperature rise at 1.0 s

Fig. 3 First step - the identification of the laser irradiation (the temperature shown in the caption is in units: K) when the measurement data contain no errors

The center of the laser spot is set to be at the point (x_c=0, y_c=0.03 m, z_c=0.03 m). The frequency of the sinusoidal component of the heating flux is f = 5 Hz. The location of the laser heating flux is shown in Fig. 3 (a). A square array of sensors 5×5 is used to "measure" the back-surface temperature. If not otherwise specified, the grid number in x direction is 9 in this paper. As the first step, a coarse and uniform grid (7×7 on yOz plane) is used to identify the location of laser spot center. The front-surface heating condition is recovered based on the back-surface temperature measurement *only*. It is assumed that the temperature measurement data are errorless. Fig. 3 (b) shows the recovered temperature on the front surface. As is seen, though the accuracy of the front-surface temperature is limited, the location of the maximum temperature rise can be well identified.

2) Second Step: Recover the Front-Surface Temperature in a Multiple Grid System

Once the location of the maximum laser heating flux is determined, we can use a sensor array, in which the sensors are arranged based on the multiple-grid pattern, to recover the front-surface temperature in a good resolution. We move the multiple-grid sensor array and make its center coincide with the location of the maximum laser heating flux identified in Fig. 3 (b).

A non-uniform mesh 10×10 is used in the center areas (red color region in Fig. 2). The three lengths in Fig. 2 are: ALI=40 mm, ALM=10 mm, ALO=10 mm. The grid lengths in the half red-color region are 5 mm, 5 mm, 10 mm, 10 mm, and 10 mm (counted from the center line of the yOz plane). There are 124 sensors totally. The sensor distribution is shown in Fig. 4. Each solid circle represents a sensor. As can be seen in Fig. 4, the sensor spacing becomes sparser from the center region to the peripheral region.

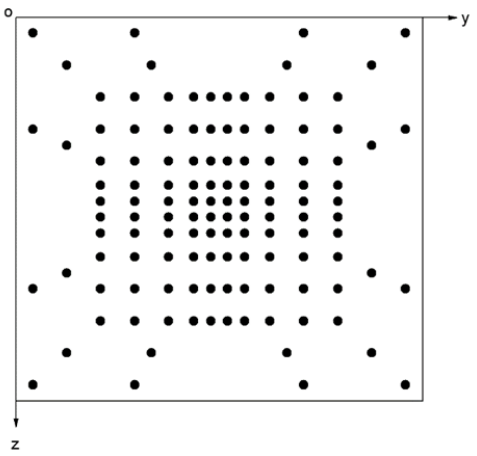

Fig. 4 Sensor distribution

Fig. 5 shows the exact and recovered temperature evolutions at laser spot center (r=0) and laser edge (r=10.6 mm) when both the temperature *and* heat flux are measured on the back surface. The RMS error is computed for each curve. As can be seen, when the measurement data do not contain

random errors, the front-surface temperature can be well recovered. The black-color dot in a rectangle at the upper-right corner indicates the location of the point where the temperature curve is plotted for.

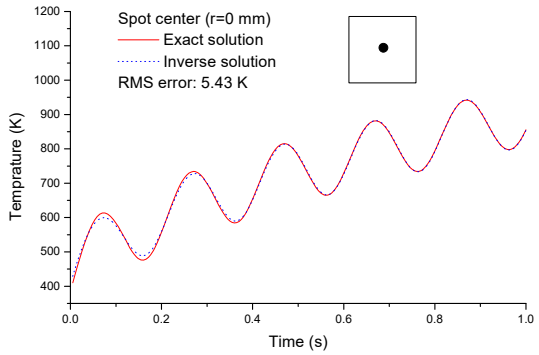

(a) at laser spot center (r=0)

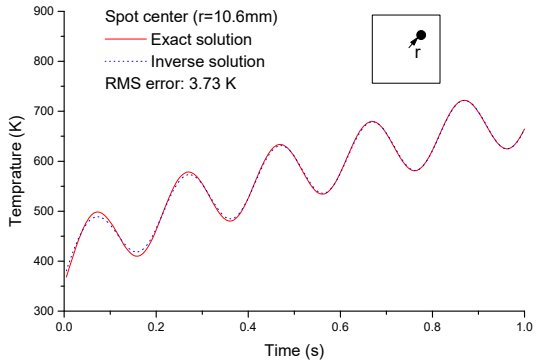

(b) at laser edge (r=10.6 mm)

Fig. 5 Exact and recovered temperature evolutions based on temperature AND heat flux measurements when the measurement data contain no errors

Fig. 6 shows the exact and recovered temperature evolutions at laser spot center (r=0) and laser edge (r=10.6 mm) when *only* the temperature is measured on the back surface. It is seen that the phase of the recovered temperature can be well recovered, but there are large errors in the amplitude of the recovered temperature. It can be concluded from Figs. 5 and 6 that more accurate inverse solutions can be obtained if both temperature AND heat flux are measured on the back surface when they can be accurately measured (i.e., no random errors).

B. Measurement Data with Random Errors

In reality, both the temperature and heat flux measurement data contain random noise. We will examine this case in this section. The simulation parameters are almost the same as those in Fig. 3 except that the frequency of the sinusoidal component of the heating flux is f = 2 Hz. The standard deviation of the random errors in temperature measurement is 2K, and the standard deviation in heat flux measurement is 5% of its maximum value. The conventional Moving Window Average method is used to smooth the measurement data.

1) First Step: Identify the Location of Laser Irradiation in a Coarse Grid System

As the first step, a coarse and uniform grid (7×7 on yOz plane) is used to identify the location of laser spot center. The front-surface temperature is recovered based on the back-surface temperature measurement only. It is assumed that the temperature measurement data contain random errors with a standard deviation of 2K. Fig. 7 shows the exact and recovered temperature on the front surface. It can be seen that the location of the maximum temperature rise can be identified.

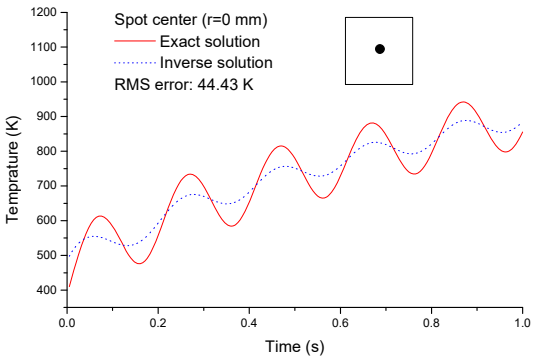

(a) at laser spot center (r=0)

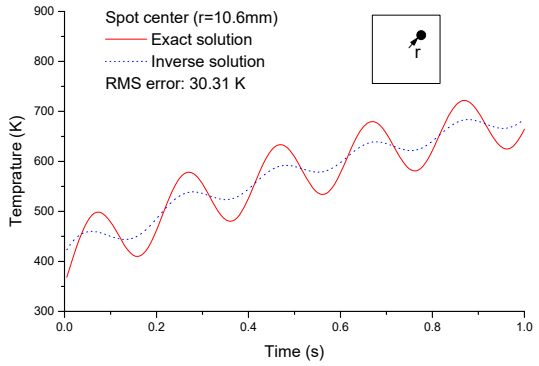

(b) at laser edge (r=10.6 mm)

Fig. 6 Exact and recovered temperature evolutions based on temperature measurement ONLY when the measurement data contain no errors

2) Second Step: Recover the Front-Surface Temperature in a Multiple Grid System

After the location of the maximum laser heating flux is determined, the multiple-grid based sensor array is used to recover the front-surface temperature. The grid size and arrangement of the multiple-grid system are the same as those in Fig. 4.

Fig. 8 shows the exact and recovered temperature evolutions at laser spot center (r=0) and laser edge (r=10.6 mm) when both the temperature *and* heat flux are measured on the back surface. As can be seen, when the measurement data have random errors, the accuracy in the front-surface temperature is severely degraded.

Fig. 9 shows the exact and recovered temperature

evolutions at laser spot center (r=0) and laser edge (r=10.6 mm) when only the temperature is measured on the back surface. It is seen that both the phase and amplitude of the front-surface temperature can be well recovered. The results from Figs. 8 and 9 clearly show that more accurate inverse solutions can be obtained if *only* the temperature is measured on the back surface when the measurement data contain random errors.

V. Conclusions

Aiming to reduce the sensor number without loss of accuracy, a two-step approach is proposed to recover the front-surface temperature using the back-surface temperature and/or heat flux measurement data. The first step involves the identification of the location of the maximum temperature rise. The second step is characterized by a sensor array based on the multiple-grid conception. Stainless steel is taken as the simulation material. Two cases are considered. One case is that the front-surface temperature is recovered based on the temperature *and* heat flux measurements on the back surface. The other case is that the front-surface temperature is recovered based on the temperature measurement *only* on the back surface. It is concluded that more accurate inverse solutions can be obtained if both temperature *and* heat flux are measured on the back surface can be accurately measured (i.e., no random errors). When the back-surface measurement data contain random noise, the noise is reduced using the Moving Window Average method. For this case, more accurate inverse solutions can be obtained if *only* the temperature is measured on the back surface.

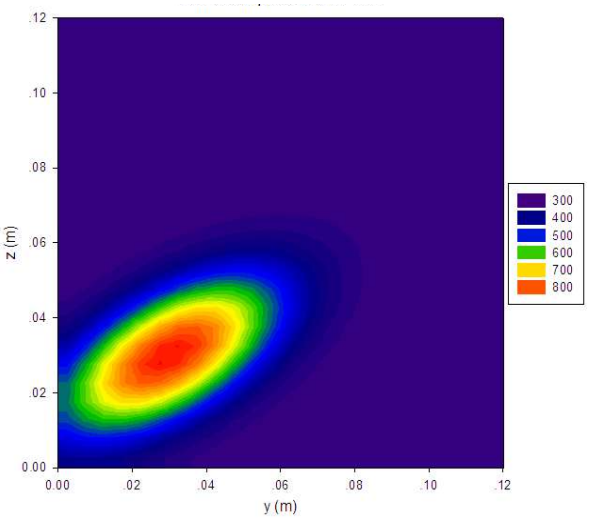

(a) The exact solution of the temperature rise at 1.0 s

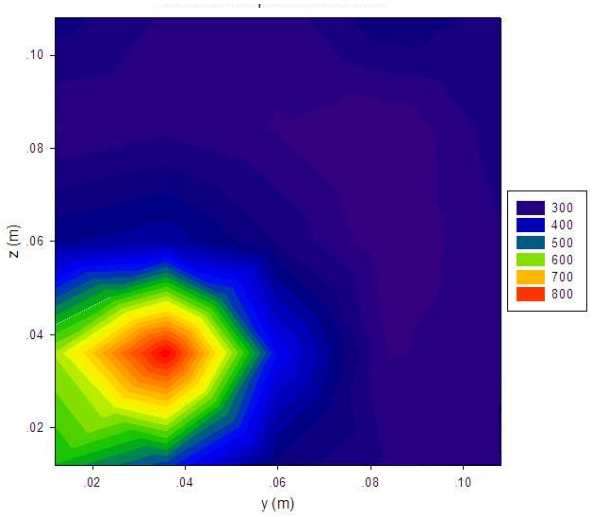

(b) The inverse solution of the temperature rise at 1.0 s

Fig. 7 First step - the identification of the laser irradiation (the temperature shown in the caption is in units: K) when the measurement data contain errors

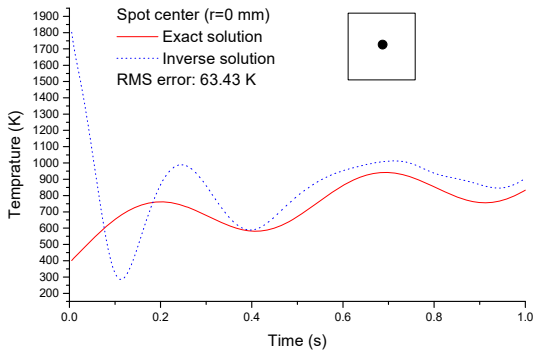

(a) at laser spot center (r=0)

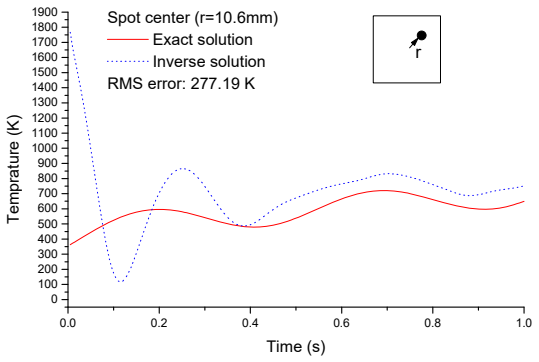

(b) at laser edge (r=10.6 mm)

Fig. 8 Exact and recovered temperature evolutions based on temperature AND heat flux measurements when the measurement data contain errors.

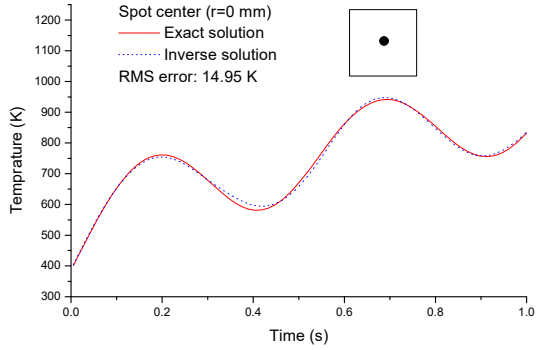

(a) at laser spot center (r=0)

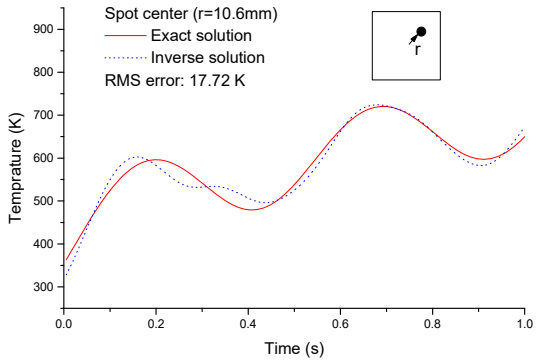

(b) at laser edge (r=10.6 mm)

Fig. 9 Exact and recovered temperature evolutions based on temperature measurement ONLY when the measurement data contain errors

REFERENCES

[1] J.V. Beck, B. Blackwell and C.R. St-Clair, *Inverse Heat Conduction: Ill Posed Problems*, Wiley, New York, (1985).

[2] O. M. Alifanov, *Inverse Heat Transfer Problems*, Springer-Verlag, Berlin/Heidelberg, (1994).

[3] M.N. Özisik and H.R.B. Orlande, *Inverse Heat Transfer: Fundamentals and Applications*, Taylor & Francis, New York, (2000).

[4] T. Lu, B. Liu and P.X. Jiang, "Inverse estimation of the inner wall temperature fluctuations in a pipe elbow," *Applied Thermal Engineering*, 31, pp. 1976-1982, (2011).

[5] M. R. Golbahar Haghighi, P. Malekzadeh, H. Rahideh, M. Vaghefi, "Inverse transient heat conduction problems of a multilayered functionally graded cylinder," *Numerical Heat Transfer, Part A: Applicaitons*, 61, pp. 717-733, (2012).

[6] A. Azimi, K. Bamdad, H. Ahmadikia, "Inverse hyperbolic heat conduction in fins with arbitrary profiles," *Numerical Heat Transfer, Part A: Applications*, 61, pp. 220-240, (2012).

[7] S.K. Kim, "Resolving the final time singularity in gradient methods for inverse heat conduction problems," *Numerical Heat Transfer, Part B: Fundamentals*, 57, pp. 74-88, (2010).

[8] M. Samaï and T. Loulou, "A comparative study of heat flux and temperature based on objective functional to solve inverse heat conduction problems," *Numerical Heat Transfer, Part B: Fundamentals*, 56, pp. 75-104, (2009).

[9] J. Zhou, Y. Zhang, J.K. Chen and Z.C. Feng, "Inverse estimation of surface heating condition in a finite slab with temperature-dependent thermophysical properties," *Heat Transfer Engineering*, vol. 32, pp. 861-875, 2011.

[10] J. Zhou, Y. Zhang, J.K. Chen and Z.C. Feng, "Inverse heat conduction in composites with pyrolysis effect and temperature-dependent thermophysical properties," ASME *Journal of Heat Transfer*, 132(3), 034502, (2010).

[11] J. Zhou, Y. Zhang, J.K. Chen and Z.C. Feng, "Inverse estimation of surface heating condition in a three-dimensional object using conjugate gradient method," *International Journal of Heat and Mass Transfer,* 53(13-14), 2643-2654, (2010).

[12] J. Zhou, Y. Zhang, J.K. Chen and Z.C. Feng, "Inverse estimation of surface temperature induced by a moving heat source in a 3-d object based on back surface temperature with random measurement errors," *Numerical Heat Transfer*, *Part A: Applications*, 61(2), 85-100, (2012).

[13] Y. Ren, Y. Zhang, J.K. Chen and Z.C. Feng, "Inverse estimation of front surface temperature of a 3-d finite slab based on back surface temperature measured at coarse grids," *Numerical Heat Transfer, Part B: Fundamentals*, 63(1), 1-17, (2013).

[14] N. Afrin, Z.C. Feng, J.K. Zhang and J.K. Chen, "Inverse estimation of front surface temperature of a locally heated plate with temperature-dependent conductivity via Kirchhoff transformation," *International Journal Thermal Sciences,* 69, 53-60, (2013).

[15] J. Zhou, Y. Zhang, J.K. Chen and Z.C. Feng, "Three-dimensional inverse heat transfer in a composite target subject to high-energy laser irradiation," ASME *Journal of Heat Transfer*, 134(11), 111201, (2012).

[16] Y. Zhang, Z.C. Feng and J.K. Chen, "Recovering the Front Surface Temperature of Metallic and Composite Targets Subject to Localized Heating via Inverse Heat Transfer Modeling," *The 15th International Heat Transfer Conference*, Kyoto, Japan, August 10-15, 2014.